

pubs.acs.org/est Article

# New Analytical Paradigm to Determine Concentration of Brown Carbon and Its Sample-by-Sample Mass Absorption Efficiency

Kezheng Liao, Yuk Ying Cheng, Sui Shing Yea, L.-W. Antony Chen, John H. Seinfeld, and Jian Zhen Yu\*



Cite This: Environ. Sci. Technol. 2024, 58, 17386–17395



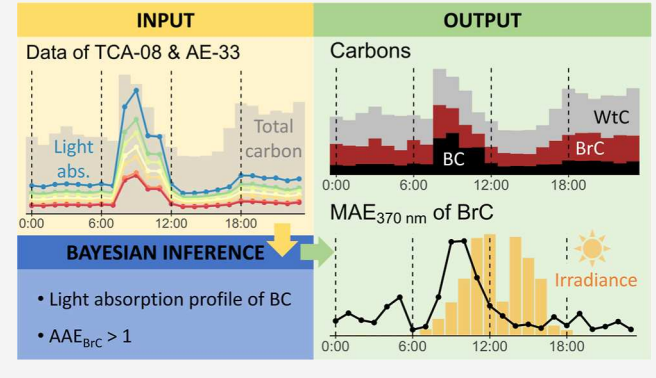
**ACCESS** I

Metrics & More

Article Recommendations

Supporting Information

ABSTRACT: Brown carbon (BrC) has a substantial direct radiative effect, but current estimates of its impact on radiative balance are highly uncertain due to a lack of measurements of its light-absorbing properties, such as mass absorption efficiency (MAE). Here, we present a new analytical paradigm based on a Bayesian inference (BI) model that takes multiwavelength aethalometer measurements and total carbon data to resolve the concentrations of black carbon and BrC, and MAEs of BrC on a sample-by-sample basis. Hourly MAEs, unattainable in previous studies, can now be calculated, enabling the first-time observation of the darkening-bleaching dynamics of BrC in response to photochemical transformation. We demonstrate the application of this BI model to analyze measurements collected over one year



(2021-2022) in Hong Kong. Diel variations in MAE<sub>370 nm</sub> of BrC reveal a darkening-to-bleaching transition occurring between 8 and 10 O'clock when the solar irradiance ranges from 30 to 400 W m<sup>-2</sup>. Furthermore, we consistently observe an increase in MAE<sub>370 nm</sub> of BrC with nitrogen oxide concentrations, suggesting the enhanced formation of nitrogenous organics. This BI model-based data analysis would bring forth a breakthrough in amassing observation data of BrC and its MAEs in diverse ambient environments and with high time resolution.

KEYWORDS: brown carbon, ambient aerosol, light absorption, aethalometer, Bayesian inference

### 1. INTRODUCTION

Carbonaceous aerosol is ubiquitous in ambient atmosphere, constituting around 20-50% of total fine particulate matter mass concentration.<sup>1,2</sup> While all carbonaceous particles scatter light to certain degrees, their light-absorbing properties can exhibit notable variations. A popular classification scheme for carbonaceous aerosol includes "white carbon (WtC), brown carbon (BrC), and black carbon (BC)". 3,4 WtC, consisting of colorless organic molecules, is generally considered nonlightabsorbing. In contrast, BC, i.e., soot-like substance, absorbs solar radiation almost indifferently within UV to visible light range.<sup>5</sup> The term BrC was introduced to describe organic components that exhibit a sharp decrease in absorption spectra from short to long wavelengths in UV-visible spectrum. 4,6 An empirical power-law formula to quantify the relationship between the mass absorption efficiency (MAE, in  $m^2\ gC^{-1}$ ) and wavelength  $(\lambda, \text{ in nm})$  for both BC and BrC is given in eq 1, incorporating material-dependent parameters K and absorption Angstrom exponent (AAE).

$$MAE = K \times \lambda^{-AAE} (AAE_{BC} \approx 1, AAE_{BrC} > 1)$$
 (1)

The AAE of bulk BC is often assumed to be around 1, resulting in its MAE being approximately a reciprocal function of wavelength. In contrast, BrC has a noticeably larger AAE,

ranging from 1.5 to 10 for BrC emitted from different sources,  $^8$  leading to a more pronounced dependence of MAE\_BrC on the wavelength. Some studies indicate that AAE\_BrC is wavelength-dependent, generally increasing toward shorter wavelengths.  $^{9,10}$  Theoretical models such as the damped harmonic oscillator model and the band gap model have been proposed to account for the relation between MAE and wavelength for BrC.  $^{11,12}$ 

BrC exerts direct impacts on solar and terrestrial radiation balance due to its light-absorbing properties as well as indirect influence on cloud formation and other microphysical processes. Recent laboratory and field studies also highlight the active role of BrC components (e.g., imidazole derivatives and humic-like substance) as photosensitizers to enhance secondary formation reactions in the atmosphere. While the significance of BrC in the global environment and climate has been well recognized in recent modeling studies, there is significant disagreement in current estimates. For instance,

Received: July 5, 2024

Revised: September 11, 2024 Accepted: September 12, 2024 Published: September 19, 2024





different studies report a wide range of global average direct radiative effect of BrC, varying from 0.03 to 0.57 W m $^{-2}$   $^{13,19-22}$ Two major causes contribute to the inadequate characterization of BrC in numeric models. First, BrC comes from a complex combination of primary combustion sources and secondary formation pathways, <sup>17,23-27</sup> giving rise to its chemical diversity and optical variability. 4 Second, the light-absorbing properties of ambient BrC continuously evolve through photochemical aging processes.<sup>28–30</sup> Due to the scarcity of observation data on BrC and its MAEs for model constrains, scientists have to rely on crude parametrization methods to estimate its emission rates, light-absorbing properties, and atmospheric aging reactions. 20,22,28 Consequently, there is an urgent need for a convenient method to quantify the BrC concentration and its varying light-absorbing properties with atmospheric transformation. Such a method would greatly facilitate obtaining observation data in both ambient and controlled environments, thereby aiding the advancement of climate models.

Among various techniques and instruments, the multiwavelength aethalometer that simultaneously measures aerosol light absorption at multiple wavelengths stands out for its cost effectiveness, labor-saving nature, and capability to provide high time-resolution data. 31,32 However, previous studies that utilize the aethalometer measurements have commonly employed the naive BrC model by assuming that the light absorption at 880 nm is entirely contributed by BC and then apportioned light absorptions to BC and BrC, which lacks the ability to determine the concentrations nor MAEs of BrC. 33,34 The MAEs of BrC are cited from other studies so that concentration of BrC can be calculated.<sup>35</sup> Recently Chen et al.<sup>36</sup> proposed a hybrid environmental receptor model (HERM), a variant of chemical mass balance (CMB) model, referred to as HERM-CMB hereafter, to quantify bulk BrC level. This model incorporates measurements of total carbon (TC) concentration and solves both the carbon mass balance equation and the light absorption balance equation at seven wavelengths. HERM-CMB uses a spectral light absorption profile instead of an AAE to characterize BrC light absorption, and is limited in two aspects. First, similar to the CMB model, HERM-CMB assumes that BrC in all observations shares the same light-absorbing profile, which may not be valid considering the dynamic optical nature of BrC.<sup>29,37</sup> Second, like other receptor models, the results of HERM-CMB can be influenced by the subjective decisions made by model users when implementing additional constraints. Insufficient documentation of these decisions can compromise reproducibility. Motivated by the increased use of Bayesian inference (BI) in air pollution research, <sup>38–40</sup> we explore BI as an alternative approach to quantify the level of BrC and its lightabsorbing properties. Different from models that estimate parameters through minimizing the objective function of gross errors (e.g., CMB and positive matrix factorization), BI allows more flexibility in constraining the parameters by defining the "prior distributions" instead of the "prior values". Specific to the case where the BI model is applied to aethalometer data along with concurrent measurements of TC concentration, it allows the MAEs of BrC to vary across individual observations as long as its MAEs and AAE fall into reasonable ranges.

In this study, we demonstrate the applicability of our novel BI model using a one-year data set from a seven-wavelength aethalometer and a total carbon analyzer (TCA) at a suburban air quality monitoring station in Hong Kong on the campus of the Hong Kong University of Science and Technology (HKUST) (see Figure S1 in the Supporting Information for

the location). Intermethod comparisons are made between the BI model and HERM–CMB, focusing on the resolved concentrations of BrC, BC, and WtC. Importantly, our BI model solves the AAE value of bulk BrC for each hour and, equivalently, its MAE values at seven different wavelengths. The availability of sample-by-sample MAEs enables us, for the first time, to examine the diurnal variations of MAE values of bulk BrC in ambient aerosol. This allows us to quantify the influences of ambient factors, such as solar irradiance and  $NO_x$  concentration, on the light-absorbing properties of BrC. Additionally, this work once again shows the unique potential of BI in general and encourages future research to extend its applications in other topics of atmospheric sciences.

#### 2. MATERIALS AND METHODS

**2.1. Sources of Observation Data.** Involved instrumentations are the total carbon analyzer (TCA-08, Magee Scientific) and the dual-spot aethalometer (AE-33, Magee Scientific), both of which are deployed at the Air Quality Research Supersite in HKUST, a typical suburban site (22.238° N, 114.263° E, Figure S1). TCA-08 analyzer flash-heats samples to convert all carbon to  $\rm CO_2$  and consequentially determines the TC concentration, while AE-33 measures the light absorption of aerosol deposited on the filter tape at seven different wavelengths, namely, 370, 470, 520, 590, 660, 880, and 950 nm. The sampling period is from July 22, 2021, to August 26, 2022. For compatibility, their readings are averaged to 1 h for data analysis. Texts below provide more information on the technical details of AE-33 in our study.

The dual-spot aethalometer AE-33 measures the light attenuation changing rate  $(\Delta ATN/\Delta t)$  as ambient aerosol accumulates at two spots on the polytetrafluoroethylene-coated (PTFE-coated) glass fiber tape (part number 8050, Magee Scientific).<sup>31</sup> The flow rates are set to 3 and 1 L min<sup>-1</sup> for two spots and are lower than the default values. This is because the ambient air in Hong Kong is quite humid, and lower flow rate allows the air to be sufficiently dehumidified in the aerosol dryer before entering AE-33. The spot with a higher flow rate is used to calculate the attenuation coefficient as per eq 2, where variables A and  $\nu$  signify the area of the aerosol deposited on the tape and the air flow rate, respectively.

$$b_{\rm ATN} = \frac{\Delta ATN}{\Delta t} \times \frac{A}{\nu} \tag{2}$$

However, raw light attenuation data from the aethalometer must be corrected after taking into account the loading effect, air flow leakage, and light scattering of the filter tape. The correction method of dual-spot aethalometer AE-33 in this study follows eq 3, where  $\zeta$  denotes the air flow leakage ratio, C for scattering, and k for loading effect constant. The leakage factor  $\zeta$  is monitored during maintenance procedures; the value of C is set to 1.57 for PTFE-coated glass fiber tape; and k is solved following the procedures in Drinovec et al.<sup>31</sup>

$$b_{\text{abs}} = b_{\text{ATN}} \times \frac{1}{1 - \zeta} \times \frac{1}{C} \times \frac{1}{1 - k \times \text{ATN}}$$
 (3)

**2.2.** Mathematical Description of the BI Model. Equations 4 and 5 are carbon mass balance and light absorption balance equations, respectively, where TC and light absorptions  $(b_{\lambda})$  at 7 wavelengths  $(\lambda_i, i = 1, 2, ..., 7)$  on the left-hand sides constitute the known information.

$$[TC] = [BC] + [BrC] + [WtC]$$
(4)

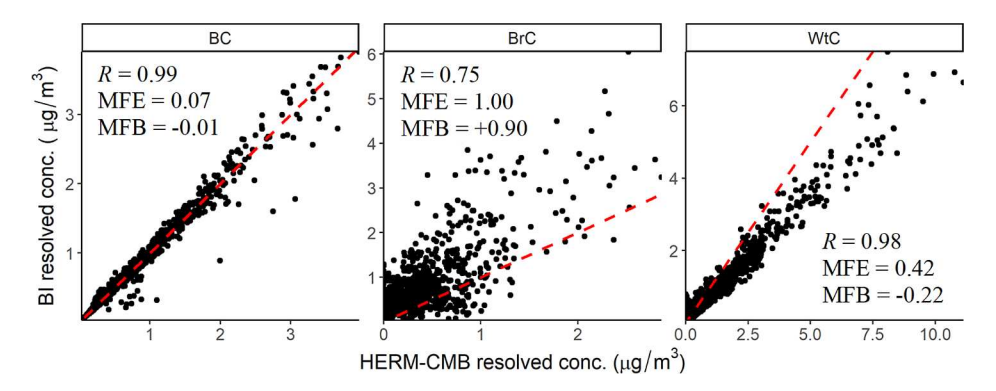


**Figure 1.** Comparisons of resolved concentrations between the BI model and the HERM–CMB model by Chen et al. (2021).<sup>36</sup> A total of 1258 hourly data from July to September 2021 are included. Red dash lines are one-to-one-ratio lines in each panel. Three model evaluation metrics, i.e., Pearson's correlation coefficient (*R*), MFE, and MFB, are provided.

$$b_{\lambda_i} = b_{\lambda_i}^{BC} + b_{\lambda_i}^{BrC} = MAE_{\lambda_i}^{BC} \times [BC] + MAE_{\lambda_i}^{BrC}$$
$$\times [BrC], \qquad i = 1, 2, ..., 7$$
(5)

First, the MAE values of BC are from reference samples following Chen et al.,  $^{36}$  whereas MAE values of BrC are described by two parameters,  $K^{\rm BrC}$  and AAE $^{\rm BrC}$  as per eq 1, so that we reach eq 6.

$$b_{\lambda_i} = \text{MAE}_{\lambda_i}^{\text{BC}} \times [\text{BC}] + (K^{\text{BrC}} \times \lambda_i^{-\text{AAE}(\text{BrC})}) \times [\text{BrC}],$$
  

$$i = 1, 2, ..., 7$$
(6)

The objective of the BI model is to derive five unknown variables (i.e., BC, BrC, WtC,  $K^{\rm BrC}$ , and AAE  $^{\rm BrC}$ ) from 8 equations for each hourly observation. Additionally, measurement errors from the aethalometer are incorporated, as described in eq 7, using a normally distributed error term. In other words, eq 7 gives the likelihood function of the BI model hereafter.

$$b_{\lambda_i} \sim N(\text{MAE}_{\lambda_i}^{\text{BC}} \times [\text{BC}] + (K^{\text{BrC}} \times \lambda_i^{-\text{AAE}(\text{BrC})})$$
$$\times [\text{BrC}], \sigma_{\lambda_i}^2), \qquad i = 1, 2, ..., 7$$
(7)

Distinct from traditional statistical models that set out to find good estimates to the "true values" of parameters, BI regards parameters of interest as random variables and aims to find their "posterior distributions" through combining two pieces of information, i.e., prior distribution and likelihood function, using Bayes' theorem.

The likelihood function in this study is fairly straightforward as per eq 7, claiming that the measurement light absorbance data are susceptible to a normally distributed error term. Additionally, the parameters of interest are the concentrations of three types of carbon and two parameters (i.e.,  $K^{\rm BrC}$  and  ${\rm AAE^{BrC}}$ ) that define the MAE- $\lambda$  relation for BrC. Texts below describe the prior distribution. An uninformative prior distribution of three types of carbon can be specified by an evenly possible three-component Dirichlet distribution scaled by the TC concentration in eq 8.

([BC], [BrC], [WtC]) 
$$\sim$$
 Dirichlet(1, 1, 1)  $\times$  [TC] (8)

The prior distribution of  $AAE^{BrC}$  is set as a two-parameter exponential distribution (eq 9) with a threshold parameter of 1, considering its physical meaning. For the base run, the scale parameter is set at 1, hence a mathematical expectation of 2.

$$AAE^{BrC} \sim 1 + exp(1) \tag{9}$$

Finally, the prior distribution of  $K^{BrC}$  is set as a normal distribution, with a mean value of  $2.7 \times 10^5$  and a standard deviation of 20% of its mean value. This mean value corresponds to a scenario when the AAE $^{BrC}$  is equal to 2 and the MAE $_{370~nm}$  of BrC is equal to 2 m $^2$  gC $^{-1}$ , which is an integer number very close to past relevant studies. We further analyzed the sensitivity of model outputs to different prior distributions and the plausibility of alternative prior distributions in Text S1.

In Bayesian analysis, when the prior distribution is not the conjugate distribution of the likelihood function, one ought to utilize alternative methods such as Markov Chain Monte Carlo (MCMC) sampling to get a numerical estimation of the posterior distribution. The fundamental idea in the MCMC algorithm is to construct a Markov Chain whose limit distribution is set to the desired posterior distribution. To achieve detailed balance with a reversible Markov Chain is the key. Specific to this paper, samples are taken from a uniform measure for simplicity. The number of total sampling steps is 10,000. The first 20% of samples are discarded for robustness, and only every 25th sample of the remaining ones is retained and analyzed. In other words, samples are thinned on the basis of 25 to avoid autocorrelation.

All algorithms used in the BI model are realized in R, a programming language for data analysis. <sup>44</sup> A sample R script for BI model together with a small data set have been uploaded onto a GitHub repository (https://github.com/CoCobalt27/Bayesian BrC, last accessed on September 3, 2024).

**2.3. Sources of Auxiliary Data.** Auxiliary data, i.e., concentrations of NO<sub>x</sub> and ozone, relative humidity (RH), and local solar irradiance, are from the Atmospheric and Environmental Database (https://envf.ust.hk/dataview, last check on February 20, 2024), launched and maintained by the Environmental Central Facility in HKUST. Solar irradiance data are recorded at the HKUST supersite, with NO<sub>x</sub> data from a neighboring site (Tseung Kwan O, 22.318° N, 114.259° E, see Figure S1), and ozone data from a background site (Tap Mun, 22.473° N, 114.358° E, see Figure S1) are used hereafter.

#### 3. RESULTS AND DISCUSSION

**3.1. Observation Data of TC Concentration and Light Absorption.** After data quality assurance and measurement correction, a total of 8934 hourly data points from TCA and aethalometer AE-33 measurements are utilized as model inputs. Figure S2 shows the number of valid data on each day during the entire period. Figure S3a,b plots the diel variations of TC concentration and aerosol light absorption at 370 nm,

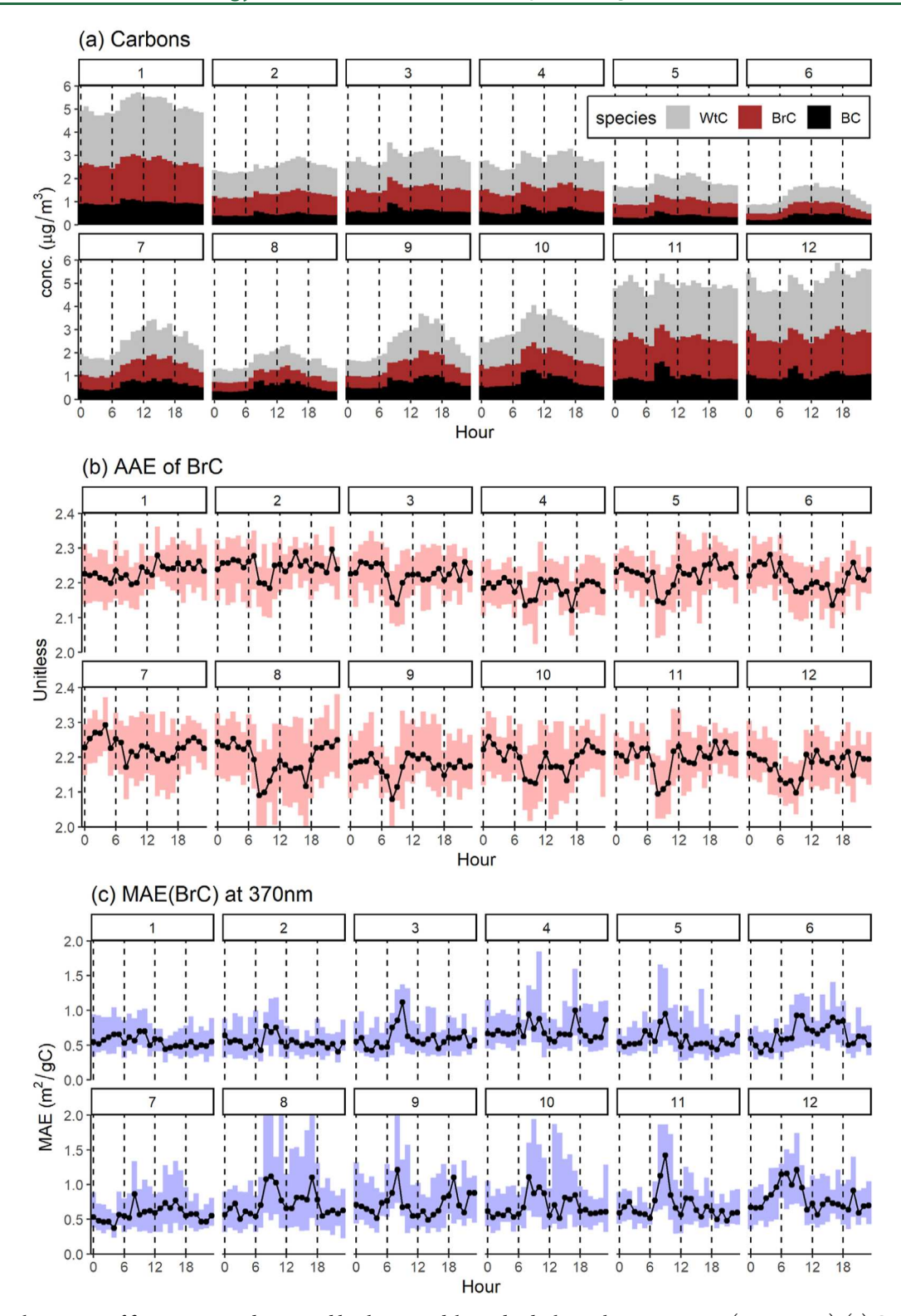


**Figure 2.** Diurnal variations of five parameters determined by the BI model in individual months over one year (2021–2022). (a) Concentrations of WtC, BrC, and BC; (b) AAE of BrC; and (c) MAE<sub>370 nm</sub> of BrC. In panels (b) and (c), dots and lines represent average values, while shadowed areas show the ranges between upper and lower quantiles. The numbers on the top of each represent months.

respectively, in every month. The wavelength at 370 nm is the shortest among the seven monitored wavelengths. At the HKUST station, TC level exhibits distinct seasonality, where an average concentration of  $\sim$ 5  $\mu$ g/m³ is recorded in winter and drops to 2  $\mu$ g/m³ in summertime (Figure S3a). The difference could be attributed to the monsoon climate and the seasonal

shift of the dominant pollution sources in Hong Kong. In winter, regional transport from the north continent brings more polluted air parcel, whereas in summer, the prevalent southerlies blow clean air from the ocean, making local emissions the primary factor. 45–47 Consequently, the diurnal patterns of the TC concentration vary across different months. Correspond-

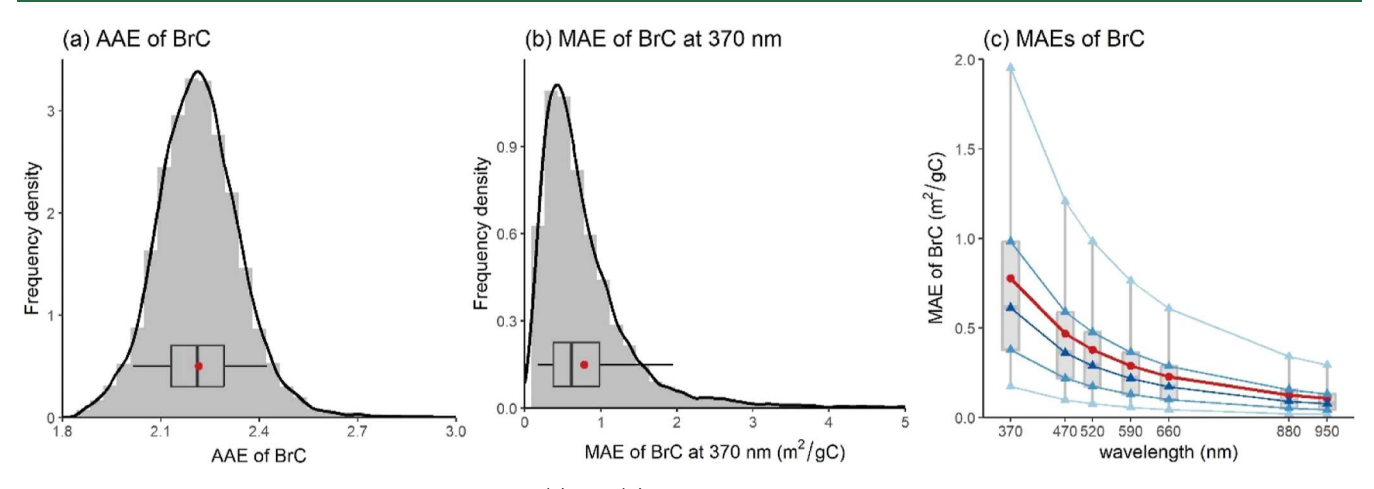


Figure 3. Distributions of AAE and MAE of BrC. Panels (a) and (b) show the frequency distributions of AAE and MAE<sub>370 nm</sub> of BrC, respectively; panel (c) visualizes the distributions of MAEs of BrC at seven wavelengths. Boxplots denote the 5%, 25%, 50%, 75%, and 95% percentiles, and red dots give the mean values.

ingly, the light absorption of bulk aerosol is higher in winter and lower in summer (Figure S3b). Notably, a distinct morning peak in light absorption is observed almost every month, which, according to our later results, can be explained by the variation in ambient BC level coupled with the evolution of the MAE of BrC. Furthermore, we compute the AAE value of bulk aerosol using light absorption measurements at seven wavelengths, 48 and its time series is shown in Figure S3c. The AAE of the bulk aerosol consistently remains larger than 1, indicating the presence of BrC throughout the year. Additionally, the disparity in AAE between winter and summer suggests that the contribution of BrC to total light absorption is more significant in the winter than in the summer. Note that time series of auxiliary data (i.e., solar irradiance, NO<sub>r</sub> level, and ozone concentration) during the study period are shown in Figure S4.

3.2. Resolved Concentrations of BC, BrC, WtC, and MAEs of BrC. The reconstructed TC concentration and total light absorptions at 7 wavelengths are validated against measurements (Figure S5), all of which exhibit highly compatible fittings with Pearson's correlation coefficients exceeding 0.99. Such compelling results serve as evidence of the BI model's excellent output data closure. At 880 nm, BI model suggests that on average around 96% of total light absorption can be attributed to BC (Figure S6a). Therefore, if the BrC model is applied to the same data set, it consistently yields lower prediction of the light absorption of BrC at 370 nm vis-à-vis the BI method by  $37.3 \pm 27.9\%$  (Figure S6b). Additionally, we compare the BI model-computed results with the HERM-CMB model by Chen et al. 36 using data from July to September 2021 (1258 hourly data) for model comparison. Table S1 in the Supporting Information lists the deduced MAEs of BC and BrC at 7 wavelengths from the HERM-CMB model. Figure 1 compares the concentrations of three carbon components derived from both the BI and HERM-CMB models. Given that both methods employ the same MAE values for BC, the resolved BC concentrations are in excellent agreement, as evidenced by a correlation coefficient of 0.99 and a mean fraction error (MFE) of 0.07. However, notable divergences and good correlations are observed in the estimated BrC and WtC between the two methods. Specifically, the BrC level derived from the BI model consistently exceeds that from the HERM-CMB model, indicated by a mean fraction bias (MFB) of +0.90 and a correlation coefficient of 0.75.

Conversely, the WtC concentration from BI is commensurately lower (MFB = -0.22, R = 0.98). The most direct cause for these discrepancies is that the BI model consistently predicts lower MAE values for BrC than those from the HERM-CMB model. For instance, the MAE $_{370~nm}$  of BrC from the HERM–CMB model is 5.40  $\pm$  0.90 m $^2$  gC $^{-1}$  (Table S1), much higher than the results from the BI model (Figures 2c and 3b). This difference can be explained by the underlying principle employed in determining the MAEs of BrC in the HERM-CMB model. The HERM-CMB is initially run to resolve the concentration of non-BC organic carbon (denoted as OC\*) and the light absorption of OC\* (denoted as  $b_{abs}^*$ ), and samples with the highest  $b_{abs}^*/[OC^*]$  ratios are used to deduce the MAEs of BrC. This results in selection of the maximum possible values for MAE of BrC in the given data set.

Time series of BC, BrC, and WtC from the BI model are visualized in Figure 2a. All three carbon types exhibit similar seasonal patterns with concentrations higher in winter and lower in summer. In most months, a morning peak of BC can be observed, which is related to the rush-hour traffic. Figure 2b displays the time series of AAE of BrC from the BI model, showing a discernible downward-upward trend in the morning for most months. In contrast, the diurnal variation of the  $MAE_{370~nm}$  of BrC shows an upward-downward shift from 6 to 12 am (Figure 2c). This inverse relationship between AAE and MAE can be quantitatively explained by calculating the derivative in eq 1 to obtain eq 10.

$$\frac{\text{dMAE}}{\text{MAE}} = -\ln \lambda \times \text{dAAE} \tag{10}$$

Given that the wavelength ( $\lambda$ ) is a value between 370 and 950 in this study, the coefficient  $(-\ln \lambda)$  in eq 10 is definitively negative. Thus, MAE and AAE exhibit opposite changes. This observation is consistent with the work by Saleh, who uses the MAE-AAE relationship to classify four types of BrC and some other studies. 49,50 They suggest that the light-absorbing property of darker BrC behaves more like BC with lower AAE. Specific to our data, considering that  $\ln \lambda$  falls between 5.91 and 6.86, we can estimate that an absolute change of +0.1 in AAE corresponds to a relative change of around -64% in MAE and vice versa. Readers can easily verify this relationship using Figure 2b,c.

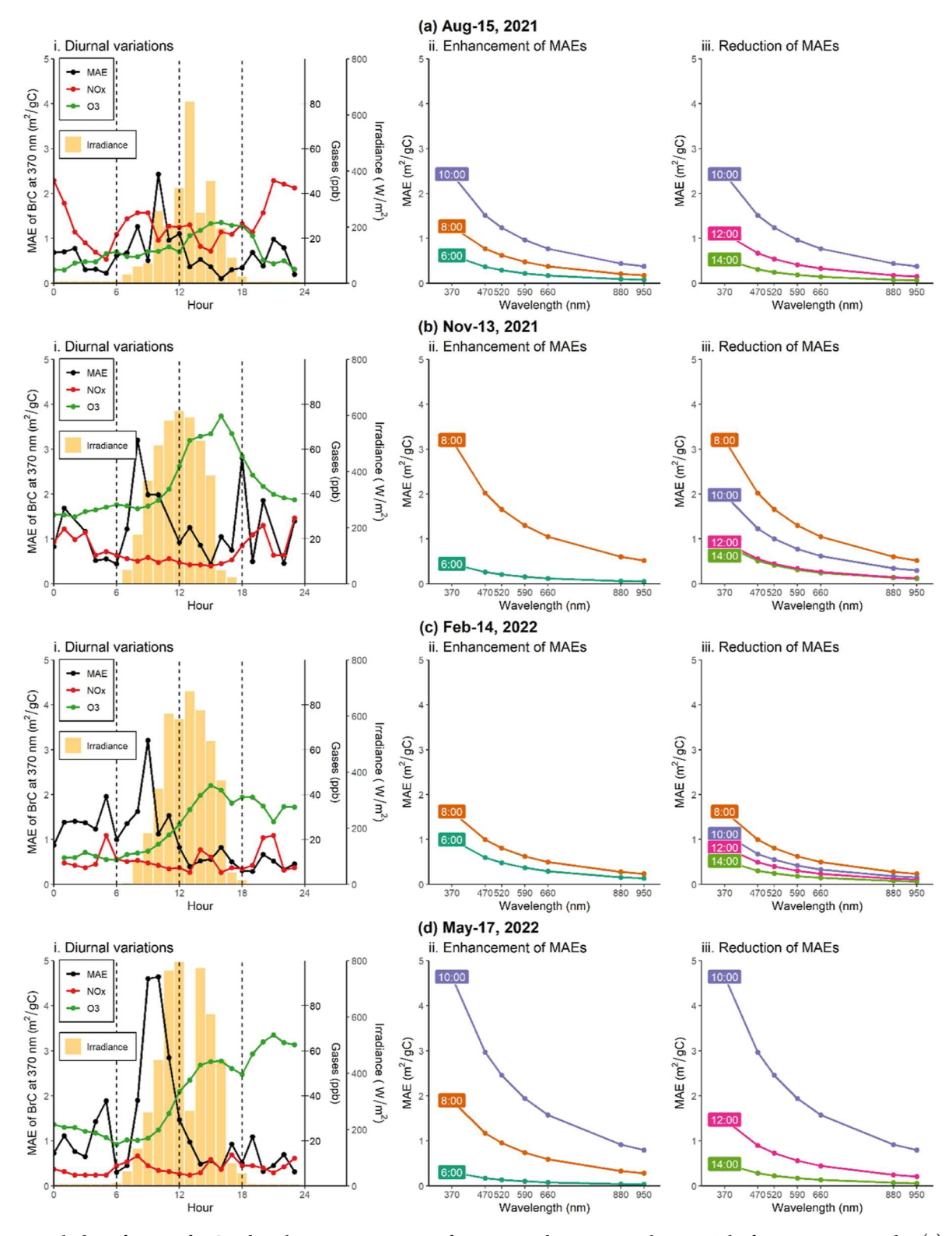


Figure 4. Hourly data of MAEs of BrC and auxiliary measurements on four separate days, one in each season. The four rows correspond to (a) Aug 15, 2021, (b) Nov 13, 2021, (c) Feb 14, 2022, and (d) May 17, 2022, respectively. Plots in the 1st column show the diurnal variations of the resolved MAE $_{370 \text{ nm}}$  of BrC (in black trace), ambient NO $_x$  concentration (in red trace), background ozone concentration (in green trace), and solar irradiance strength (in yellow bar). Plots in the 2nd column show the enhancement of MAEs of BrC at even-numbered hours in the daytime, whereas plots in the 3rd column demonstrate the reduction of MAEs.

Regarding the MAEs of BrC, Figure 3 displays the frequency distributions of all the 8934 hourly MAE $_{370~\rm nm}$  and AAE data, as well as the wavelength-dependent MAE curves corresponding to the 5th, 25th, 50th, 75th, and 95th percentile values. The overall

average MAE $_{370~nm}$  is  $0.78\pm0.62~m^2~gC^{-1}$ , while the 5th to 95th percentile spans the range of  $0.17-1.95~m^2~gC^{-1}$  and the 25th to 75th percentile spans the range of  $0.38-0.98~m^2~gC^{-1}$ . In comparison, previous relevant studies have deduced MAE $_{365~nm}$ 

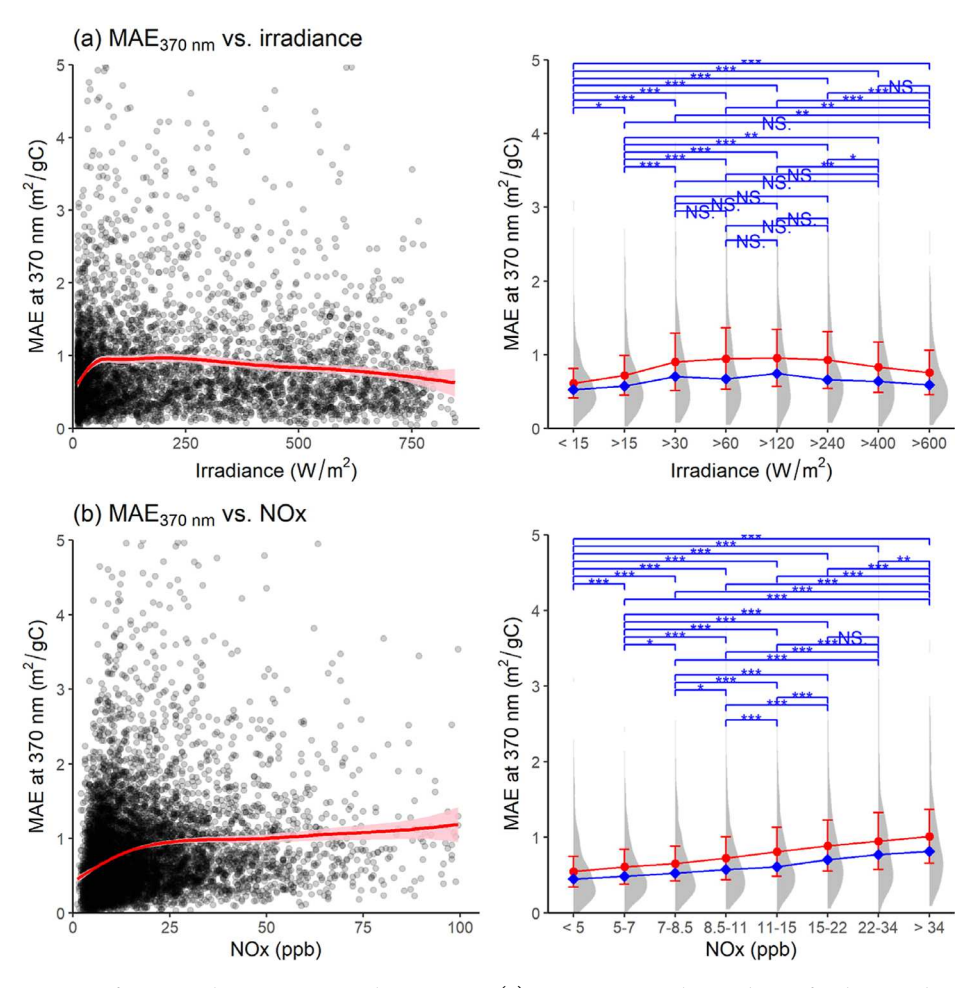


Figure 5. Resolved MAE<sub>370 nm</sub> of BrC vs other environmental parameters. (a) MAE<sub>370 nm</sub> vs solar irradiance for daytime data and (b) MAE<sub>370 nm</sub> vs NO<sub>x</sub> concentration. Each scatter plot is accompanied by an empirical fitting (red line) using generalized additive model, with a shadowed pink area showing the 95% confidence interval. Raw data are further binned into 8 groups with roughly equal amounts of data points in half-violin plots on the right. Red dots, error bars, and lines represent the mean value, the standard deviation, and the trend, respectively. Blue dots and lines show the median values and their trend. The nonparametric Wilcoxon test is used to test the differences among different bins (\*\*\*p < 0.001, \*\*p < 0.05, and NS for nonsignificant).

values of 0.68–1.0 m² gC $^{-1}$  for water-soluble organic carbon in the nearby Guangzhou  $^{41,43}$  and 1.2 m² gC $^{-1}$  for organic carbon in Hong Kong.  $^{42}$  On the other hand, the AAE of BrC, as a measure of the spectral absorption dependence, is expected to vary as BrC undergoes transformation. The overall average AAE $_{\rm BrC}$  of all the 8934 hourly measurements is 2.21  $\pm$  0.13, implying the prevalent influence of strongly to moderately light-absorbing BrC components from primary combustion sources.  $^{8,28}$ 

**3.3. Factors That Influence the MAEs of BrC.** Importantly, from the perspective of atmospheric chemistry, the variations of AAE and MAE of BrC indicate the dynamic nature of its light-absorbing properties, which have been reported by numerous studies to be associated with photochemical processes and other secondary reactions. <sup>29,37,51,52</sup> For the purpose of demonstration, we select data on 4 sunny days as examples, one each in a different season, and visualize them in Figure 4. The plots show changes of the MAE<sub>370 nm</sub> of BrC, MAEs at 7 wavelengths during even-numbered hours in the daytime, and auxiliary data (i.e., solar irradiance strength, NO<sub>x</sub>, and ozone). Throughout these 4 days, the MAE<sub>370 nm</sub> of BrC was below 2 m<sup>2</sup> gC<sup>-1</sup> for most of the time. A noticeable darkening-bleaching shift occurred in the morning on all 4 days, resulting in a maximal MAE<sub>370 nm</sub> value appearing between 8 and 10 am. The

most significant change was observed on the morning of May 17, 2022 (Figure 4d), when the MAE  $_{\rm 370~nm}$  of BrC rapidly increased from 0.30 m² gC $^{-1}$  at 6:00 to 4.64 m² gC $^{-1}$  at 10:00 and then rapidly dropped to 1.47 m² gC $^{-1}$  at noon. Notably, this particular day exhibited the highest solar irradiance among the 4 days, reaching 796 W m $^{-2}$  at 12 O'clock.

To further understand the relationship between the MAE<sub>370 nm</sub> of BrC and ambient solar irradiance, we present a scatter plot together with a half-violin plot of all daytime data (consisting of 4583 hourly data points) in Figure 5. The left panel of Figure 5a shows a nonparametric empirical fitting curve between these two variables, generated using a general additive model with cubic splines as the smoothing technique.<sup>53</sup> The curve indicates that as solar irradiance increases the MAE<sub>370 nm</sub> of BrC initially rises but then steadily declines once the irradiance reaches approximately 67 W m<sup>-2</sup>. This hypothesis is further supported by the half-violin plot in the right panel of Figure 5a, where the data are binned into 8 groups with roughly equal numbers of data points. A robust nonparametric test, namely, Wilcoxon test, is used to detect the differences between all pairs of groups.<sup>54</sup> The findings from Figure 5a indicate that the MAE<sub>370 nm</sub> data of the middle four groups, corresponding to irradiance levels between 30 and 400 W m<sup>-2</sup>, are not significantly different from each other but significantly higher

than the other four groups at both ends. In short, solar irradiance acts as an influential factor in the MAE of BrC. Increasing solar irradiance initially leads to darkening of BrC, followed by a subsequent bleaching effect.

Similar analyses have been conducted for  $NO_x$  (Figure 5b), RH (Figure S7a), and ozone (Figure S7b). Figure 5b reveals that an increase in ambient  $NO_x$  level leads to a monotonic and statistically significant rise in the MAE<sub>370 nm</sub> of BrC, potentially attributable to the enhanced formation of nitrogen-containing organic compounds, which are major constituents of BrC. Such phenomena are in accordance with those in past studies.  $^{51,52,55}$ 

Furthermore, it is noteworthy that the MAE of bulk BrC is influenced by various intertwined factors. Some factors, for instance, changes in the dominant emission sources of primary BrC, the reactions of nitrogen-absent BrC compounds, and gasparticle partitioning shifted by temperature, are not discussed in this study. To quantify effects from concurrent processes that influence the MAEs of BrC components, we recommend joint chemical speciation measurement of BrC, which might offer more source-specific insights. However, the analyses presented above regarding the characteristics of the MAEs of BrC demonstrate consistency with established knowledge in atmospheric chemistry; they also reinforce the integrity of the BI model and its ability to determine the concentrations of three carbon types and the MAEs of BrC on a sample-by-sample basis.

**3.4. Perspective.** The application of the BI approach to TC and multiwavelength aethalometer measurements represents a novel analytical paradigm for determining concentrations of BrC, its light absorption properties (i.e., MAE and AAE), and concentrations of BC and WtC on a sample-by-sample basis. The ability to quickly resolve MAEs for individual samples enables the observation of diel variations of MAEs of bulk BrC in response to photochemical and other secondary reactions as they modify the light-absorbing properties of BrC. This unique feature is not available in past methodologies, such as spectrometer measurement coupled with labor-intensive solvent extraction, the BrC model, or the HERM-CMB model, all of which suffer from their inherent method rigidity. Specifically, the BrC model can only determine the overall light absorptions caused by BrC, but even this is biased, as illustrated in Figure S6, because the model is limited by its simplistic assumption that light absorption at long wavelengths is solely contributed to BC. On the other hand, the HERM-CMB model utilizes a brownness index  $(\gamma_{Br})$ , <sup>36</sup> defined as the [BrC]-to-[OC\*] ratio, with BrC calculated using a fixed light absorption profile based on 20 samples with the highest  $b_{abs}^*/[OC^*]$  ratios. Although the brownness index can explain the light absorption decrease of BrC by its concentration, it is incapable of showing the dynamic nature of MAEs or the darkening of OC\*. Unlike HERM-CMB model, the BI method does not assume a predefined MAE profile, and the MAE profile is independently derived on a persample basis, thus permitting the observation of either darkening or bleaching of BrC. It is also noteworthy that the BI method couples TC measurements with light absorption readings, thus enabling the derivation of mass concentration of BC and BrC. This moves beyond the conventional estimate of equivalent BC,56 which is derived solely based on optical absorption measurement and in which light absorptions of BrC are not explicitly accounted for (Figure S6).

The ability to track MAEs on a per-sample basis makes it possible to inspect the associations between MAE and various ambient factors as well as the impact of episodic emissions or secondary processes on modifying BrC. In controlled laboratory

studies (e.g., chamber experiments and source-oriented research) focusing on specific BrC components, the BI method provides a convenient way to monitor changes in concentration of BrC and MAEs. Quantifying such information is invaluable for assessing the formation and aging rates of BrC. Thus, the new method opens the door to readily collecting large data sets of MAEs and AAE for BrC in various ambient locations and with high time resolution. This would provide the necessary data foundation for accurately parametrizing the concentration and light-absorbing properties of BrC in climate and visibility models, which currently assume static light absorption efficiencies.

### ASSOCIATED CONTENT

#### **Data Availability Statement**

All data required to examine the conclusions in this paper are present in the paper and/or the Supporting Information. Additional data related to this paper will be available upon request.

## Supporting Information

The Supporting Information is available free of charge at https://pubs.acs.org/doi/10.1021/acs.est.4c06831.

Sensitivity analyses of the BI model; light absorption profiles for the previously reported hybrid model; map of air quality stations discussed in this study; data availability calendar of used data set; diurnal variations of model inputs and auxiliary data; comparison between reconstructed data and measurements; resolved MAE of BrC vs  $NO_x$  level; and resolved MAE of BrC vs ozone concentration (PDF)

#### AUTHOR INFORMATION

#### **Corresponding Author**

Jian Zhen Yu — Department of Chemistry, The Hong Kong University of Science and Technology, Kowloon, Hong Kong 999077, China; Division of Environment and Sustainability, The Hong Kong University of Science and Technology, Kowloon, Hong Kong 999077, China; ⊙ orcid.org/0000-0002-6165-6500; Email: jian.yu@ust.hk

## Authors

Kezheng Liao — Department of Chemistry, The Hong Kong University of Science and Technology, Kowloon, Hong Kong 999077, China; Division of Environment and Sustainability, The Hong Kong University of Science and Technology, Kowloon, Hong Kong 999077, China; ⊙ orcid.org/0000-0003-0570-6929

Yuk Ying Cheng — Department of Chemistry, The Hong Kong University of Science and Technology, Kowloon, Hong Kong 999077, China

Sui Shing Yea – Division of Environment and Sustainability, The Hong Kong University of Science and Technology, Kowloon, Hong Kong 999077, China

L.-W. Antony Chen — Department of Environmental and Occupational Health, School of Public Health, University of Nevada, Las Vegas, Las Vegas, Nevada 89154, United States; Division of Atmospheric Sciences, Desert Research Institute, Reno, Nevada 89512, United States; orcid.org/0000-0002-2311-7506

John H. Seinfeld – Division of Chemistry and Chemical Engineering, California Institute of Technology, Pasadena, California 91125, United States; o orcid.org/0000-0003-

Complete contact information is available at: https://pubs.acs.org/10.1021/acs.est.4c06831

#### **Notes**

The authors declare no competing financial interest.

#### ACKNOWLEDGMENTS

This work was supported by the Hong Kong Research Grants Council (R6011-18, GRF-16215524) and the Hong Kong University of Science and Technology (3030\_059 and AIS Support Fund for Collaborative Interdisciplinary Projects). In addition, L.-W. A. Chen's contribution is supported by the National Science Foundation under Grant Nos. OIA-2148788 and AGS-2026824.

#### REFERENCES

- (1) Jacobson, M. C.; Hansson, H.-C.; Noone, K. J.; Charlson, R. J. Organic Atmospheric Aerosols: Review and State of the Science. *Rev. Geophys.* **2000**, 38 (2), 267–294.
- (2) Kanakidou, M.; Seinfeld, J. H.; Pandis, S. N.; Barnes, I.; Dentener, F. J.; Facchini, M. C.; Van Dingenen, R.; Ervens, B.; Nenes, A.; Nielsen, C. J.; Swietlicki, E.; Putaud, J. P.; Balkanski, Y.; Fuzzi, S.; Horth, J.; Moortgat, G. K.; Winterhalter, R.; Myhre, C. E. L.; Tsigaridis, K.; Vignati, E.; Stephanou, E. G.; Wilson, J. Organic Aerosol and Global Climate Modelling: A Review. *Atmos. Chem. Phys.* **2005**, 5 (4), 1053–1123
- (3) Andreae, M. O.; Gelencsér, A. Black Carbon or Brown Carbon? The Nature of Light-Absorbing Carbonaceous Aerosols. *Atmos. Chem. Phys.* **2006**, *6* (10), 3131–3148.
- (4) Laskin, A.; Laskin, J.; Nizkorodov, S. A. Chemistry of Atmospheric Brown Carbon. *Chem. Rev.* **2015**, *115* (10), 4335–4382.
- (5) Bond, T. C.; Doherty, S. J.; Fahey, D. W.; Forster, P. M.; Berntsen, T.; DeAngelo, B. J.; Flanner, M. G.; Ghan, S.; Kärcher, B.; Koch, D.; Kinne, S.; Kondo, Y.; Quinn, P. K.; Sarofim, M. C.; Schultz, M. G.; Schulz, M.; Venkataraman, C.; Zhang, H.; Zhang, S.; Bellouin, N.; Guttikunda, S. K.; Hopke, P. K.; Jacobson, M. Z.; Kaiser, J. W.; Klimont, Z.; Lohmann, U.; Schwarz, J. P.; Shindell, D.; Storelvmo, T.; Warren, S. G.; Zender, C. S. Bounding the Role of Black Carbon in the Climate System: A Scientific Assessment. *J. Geophys. Res.: Atmos.* 2013, 118 (11), 5380–5552.
- (6) Ramanathan, V.; Li, F.; Ramana, M. V.; Praveen, P. S.; Kim, D.; Corrigan, C. E.; Nguyen, H.; Stone, E. A.; Schauer, J. J.; Carmichael, G. R.; Adhikary, B.; Yoon, S. C. Atmospheric Brown Clouds: Hemispherical and Regional Variations in Long-Range Transport, Absorption, and Radiative Forcing. *J. Geophys. Res.: Atmos.* 2007, 112 (D22), D22S21.
- (7) Moosmüller, H.; Chakrabarty, R. K.; Ehlers, K. M.; Arnott, W. P. Absorption Ångström Coefficient, Brown Carbon, and Aerosols: Basic Concepts, Bulk Matter, and Spherical Particles. *Atmos. Chem. Phys.* **2011**, *11* (3), 1217–1225.
- (8) Saleh, R. From Measurements to Models: Toward Accurate Representation of Brown Carbon in Climate Calculations. *Curr. Pollut. Rep.* **2020**, *6* (2), 90–104.
- (9) Rathod, T.; Sahu, S. K.; Tiwari, M.; Yousaf, A.; Bhangare, R. C.; Pandit, G. G. Light Absorbing Properties of Brown Carbon Generated from Pyrolytic Combustion of Household Biofuels. *Aerosol Air Qual. Res.* **2017**, *17* (1), 108–116.
- (10) Zeng, L.; Dibb, J.; Scheuer, E.; Katich, J. M.; Schwarz, J. P.; Bourgeois, I.; Peischl, J.; Ryerson, T.; Warneke, C.; Perring, A. E.; Diskin, G. S.; DiGangi, J. P.; Nowak, J. B.; Moore, R. H.; Wiggins, E. B.; Pagonis, D.; Guo, H.; Campuzano-Jost, P.; Jimenez, J. L.; Xu, L.; Weber, R. J. Characteristics and Evolution of Brown Carbon in Western United States Wildfires. *Atmos. Chem. Phys.* **2022**, *22* (12), 8009–8036.

- (11) Demtröder, W. Laser Spectroscopy: Basic Concepts and Instrumentation; Advanced Texts in Physics; Springer: Berlin, Heidelberg, 2003.
- (12) Sun, H.; Biedermann, L.; Bond, T. C. Color of Brown Carbon: A Model for Ultraviolet and Visible Light Absorption by Organic Carbon Aerosol. *Geophys. Res. Lett.* **2007**, 34 (17), 029797.
- (13) Feng, Y.; Ramanathan, V.; Kotamarthi, V. R. Brown Carbon: A Significant Atmospheric Absorber of Solar Radiation? *Atmos. Chem. Phys.* **2013**, *13* (17), 8607–8621.
- (14) Alexander, D. T. L.; Crozier, P. A.; Anderson, J. R. Brown Carbon Spheres in East Asian Outflow and Their Optical Properties. *Science* **2008**, 321 (5890), 833–836.
- (15) Yan, J.; Wang, X.; Gong, P.; Wang, C.; Cong, Z. Review of Brown Carbon Aerosols: Recent Progress and Perspectives. *Sci. Total Environ.* **2018**, *634*, 1475–1485.
- (16) Rossignol, S.; Aregahegn, K. Z.; Tinel, L.; Fine, L.; Nozière, B.; George, C. Glyoxal Induced Atmospheric Photosensitized Chemistry Leading to Organic Aerosol Growth. *Environ. Sci. Technol.* **2014**, 48 (6), 3218–3227.
- (17) Zhang, R.; Gen, M.; Liang, Z.; Li, Y. J.; Chan, C. K. Photochemical Reactions of Glyoxal during Particulate Ammonium Nitrate Photolysis: Brown Carbon Formation, Enhanced Glyoxal Decay, and Organic Phase Formation. *Environ. Sci. Technol.* **2022**, *56* (3), 1605–1614.
- (18) Li, S.; Jiang, X.; Roveretto, M.; George, C.; Liu, L.; Jiang, W.; Zhang, Q.; Wang, W.; Ge, M.; Du, L. Photochemical Aging of Atmospherically Reactive Organic Compounds Involving Brown Carbon at the Air—Aqueous Interface. *Atmos. Chem. Phys.* **2019**, *19* (15), 9887—9902.
- (19) Hammer, M. S.; Martin, R. V.; van Donkelaar, A.; Buchard, V.; Torres, O.; Ridley, D. A.; Spurr, R. J. D. Interpreting the Ultraviolet Aerosol Index Observed with the OMI Satellite Instrument to Understand Absorption by Organic Aerosols: Implications for Atmospheric Oxidation and Direct Radiative Effects. *Atmos. Chem. Phys.* **2016**, *16* (4), 2507–2523.
- (20) Zhang, A.; Wang, Y.; Zhang, Y.; Weber, R. J.; Song, Y.; Ke, Z.; Zou, Y. Modeling the Global Radiative Effect of Brown Carbon: A Potentially Larger Heating Source in the Tropical Free Troposphere than Black Carbon. *Atmos. Chem. Phys.* **2020**, 20 (4), 1901–1920.
- (21) Lin, G.; Penner, J. E.; Flanner, M. G.; Sillman, S.; Xu, L.; Zhou, C. Radiative Forcing of Organic Aerosol in the Atmosphere and on Snow: Effects of SOA and Brown Carbon. *J. Geophys. Res.: Atmos.* **2014**, *119* (12), 7453–7476.
- (22) Wang, X.; Heald, C. L.; Liu, J.; Weber, R. J.; Campuzano-Jost, P.; Jimenez, J. L.; Schwarz, J. P.; Perring, A. E. Exploring the Observational Constraints on the Simulation of Brown Carbon. *Atmos. Chem. Phys.* **2018**, *18* (2), 635–653.
- (23) Tian, J.; Wang, Q.; Ni, H.; Wang, M.; Zhou, Y.; Han, Y.; Shen, Z.; Pongpiachan, S.; Zhang, N.; Zhao, Z.; Zhang, Q.; Zhang, Y.; Long, X.; Cao, J. Emission Characteristics of Primary Brown Carbon Absorption From Biomass and Coal Burning: Development of an Optical Emission Inventory for China. *J. Geophys. Res.: Atmos.* **2019**, *124* (3), 1879–
- (24) Zhang, Y.; Albinet, A.; Petit, J.-E.; Jacob, V.; Chevrier, F.; Gille, G.; Pontet, S.; Chrétien, E.; Dominik-Sègue, M.; Levigoureux, G.; Močnik, G.; Gros, V.; Jaffrezo, J.-L.; Favez, O. Substantial Brown Carbon Emissions from Wintertime Residential Wood Burning over France. Sci. Total Environ. 2020, 743, 140752.
- (25) Tang, J.; Li, J.; Su, T.; Han, Y.; Mo, Y.; Jiang, H.; Cui, M.; Jiang, B.; Chen, Y.; Tang, J.; Song, J.; Peng, P.; Zhang, G. Molecular Compositions and Optical Properties of Dissolved Brown Carbon in Biomass Burning, Coal Combustion, and Vehicle Emission Aerosols Illuminated by Excitation—Emission Matrix Spectroscopy and Fourier Transform Ion Cyclotron Resonance Mass Spectrometry Analysis. *Atmos. Chem. Phys.* **2020**, *20* (4), 2513–2532.
- (26) Updyke, K. M.; Nguyen, T. B.; Nizkorodov, S. A. Formation of Brown Carbon via Reactions of Ammonia with Secondary Organic Aerosols from Biogenic and Anthropogenic Precursors. *Atmos. Environ.* **2012**, *63*, 22–31.

- (27) Bones, D. L.; Henricksen, D. K.; Mang, S. A.; Gonsior, M.; Bateman, A. P.; Nguyen, T. B.; Cooper, W. J.; Nizkorodov, S. A. Appearance of Strong Absorbers and Fluorophores in Limonene-O3 Secondary Organic Aerosol Due to NH4+-Mediated Chemical Aging over Long Time Scales. *J. Geophys. Res.: Atmos.* **2010**, *115* (D5), 012864.
- (28) Saleh, R.; Robinson, E. S.; Tkacik, D. S.; Ahern, A. T.; Liu, S.; Aiken, A. C.; Sullivan, R. C.; Presto, A. A.; Dubey, M. K.; Yokelson, R. J.; Donahue, N. M.; Robinson, A. L. Brownness of Organics in Aerosols from Biomass Burning Linked to Their Black Carbon Content. *Nat. Geosci.* **2014**, *7* (9), 647–650.
- (29) Zhong, M.; Jang, M. Dynamic Light Absorption of Biomass-Burning Organic Carbon Photochemically Aged under Natural Sunlight. *Atmos. Chem. Phys.* **2014**, *14* (3), 1517–1525.
- (30) Schnitzler, E. G.; Gerrebos, N. G. A.; Carter, T. S.; Huang, Y.; Heald, C. L.; Bertram, A. K.; Abbatt, J. P. D. Rate of Atmospheric Brown Carbon Whitening Governed by Environmental Conditions. *Proc. Natl. Acad. Sci. U.S.A.* 2022, 119 (38), No. e2205610119.
- (31) Drinovec, L.; Močnik, G.; Zotter, P.; Prévôt, A. S. H.; Ruckstuhl, C.; Coz, E.; Rupakheti, M.; Sciare, J.; Müller, T.; Wiedensohler, A.; Hansen, A. D. A. The "Dual-Spot" Aethalometer: An Improved Measurement of Aerosol Black Carbon with Real-Time Loading Compensation. *Atmos. Meas. Tech.* **2015**, *8* (5), 1965–1979.
- (32) Collaud Coen, M.; Weingartner, E.; Apituley, A.; Ceburnis, D.; Fierz-Schmidhauser, R.; Flentje, H.; Henzing, J. S.; Jennings, S. G.; Moerman, M.; Petzold, A.; Schmid, O.; Baltensperger, U. Minimizing Light Absorption Measurement Artifacts of the Aethalometer: Evaluation of Five Correction Algorithms. *Atmos. Meas. Tech.* **2010**, 3 (2), 457–474.
- (33) Olson, M. R.; Victoria Garcia, M.; Robinson, M. A.; Van Rooy, P.; Dietenberger, M. A.; Bergin, M.; Schauer, J. J. Investigation of Black and Brown Carbon Multiple-wavelength-dependent Light Absorption from Biomass and Fossil Fuel Combustion Source Emissions. *J. Geophys. Res.: Atmos.* **2015**, *120* (13), 6682–6697.
- (34) Liu, S.; Luo, T.; Zhou, L.; Song, T.; Wang, N.; Luo, Q.; Huang, G.; Jiang, X.; Zhou, S.; Qiu, Y.; Yang, F. Vehicle Exhausts Contribute High Near-UV Absorption through Carbonaceous Aerosol during Winter in a Fast-Growing City of Sichuan Basin, China. *Environ. Pollut.* **2022**, 312, 119966.
- (35) Cheng, Y.; Liu, C.; Wang, J.; Wang, J.; Zhang, Z.; Chen, L.; Ge, D.; Zhu, C.; Wang, J.; Ding, A. An Observation-Constrained Estimation of Brown Carbon Aerosol Direct Radiative Effects. *Atmos. Chem. Phys.* **2024**, 24 (5), 3065–3078.
- (36) Chen, L.-W. A.; Chow, J. C.; Wang, X.; Cao, J.; Mao, J.; Watson, J. G. Brownness of Organic Aerosol over the United States: Evidence for Seasonal Biomass Burning and Photobleaching Effects. *Environ. Sci. Technol.* **2021**, *55* (13), 8561–8572.
- (37) Li, C.; He, Q.; Schade, J.; Passig, J.; Zimmermann, R.; Meidan, D.; Laskin, A.; Rudich, Y. Dynamic Changes in Optical and Chemical Properties of Tar Ball Aerosols by Atmospheric Photochemical Aging. *Atmos. Chem. Phys.* **2019**, *19* (1), 139–163.
- (38) Andersson, A.; Deng, J.; Du, K.; Zheng, M.; Yan, C.; Sköld, M.; Gustafsson, O. ∴ Regionally-Varying Combustion Sources of the January 2013 Severe Haze Events over Eastern China. *Environ. Sci. Technol.* 2015, 49 (4), 2038–2043.
- (39) Zong, Z.; Wang, X.; Tian, C.; Chen, Y.; Fang, Y.; Zhang, F.; Li, C.; Sun, J.; Li, J.; Zhang, G. First Assessment of NO<sub>x</sub> Sources at a Regional Background Site in North China Using Isotopic Analysis Linked with Modeling. *Environ. Sci. Technol.* **2017**, *51* (11), 5923–5931.
- (40) Liao, K.; Wang, Q.; Wang, S.; Yu, J. Z. Bayesian Inference Approach to Quantify Primary and Secondary Organic Carbon in Fine Particulate Matter Using Major Species Measurements. *Environ. Sci. Technol.* **2023**, *57* (13), 5169–5179.
- (41) Fan, X.; Wei, S.; Zhu, M.; Song, J.; Peng, P. Comprehensive Characterization of Humic-like Substances in Smoke PM<sub>2.5</sub> Emitted from the Combustion of Biomass Materials and Fossil Fuels. *Atmos. Chem. Phys.* **2016**, *16* (20), 13321–13340.

- (42) Zhang, Q.; Shen, Z.; Zhang, L.; Zeng, Y.; Ning, Z.; Zhang, T.; Lei, Y.; Wang, Q.; Li, G.; Sun, J.; Westerdahl, D.; Xu, H.; Cao, J. Investigation of Primary and Secondary Particulate Brown Carbon in Two Chinese Cities of Xi'an and Hong Kong in Wintertime. *Environ. Sci. Technol.* **2020**, *54* (7), 3803–3813.
- (43) Mo, Y.; Li, J.; Cheng, Z.; Zhong, G.; Zhu, S.; Tian, C.; Chen, Y.; Zhang, G. Dual Carbon Isotope-Based Source Apportionment and Light Absorption Properties of Water-Soluble Organic Carbon in PM2.5 Over China. *J. Geophys. Res.: Atmos.* **2021**, *126* (8), No. e2020JD033920.
- (44) R Core Team R. The R Project for Statistical Computing. https://www.r-project.org/ (accessed Nov 6, 2023).
- (45) Qin, Y.; Chan, C. K.; Chan, L. Y. Characteristics of Chemical Compositions of Atmospheric Aerosols in Hong Kong: Spatial and Seasonal Distributions. *Sci. Total Environ.* **1997**, *206* (1), 25–37.
- (46) Yu, J. Z.; Tung, J. W. T.; Wu, A. W. M.; Lau, A. K. H.; Louie, P. K.-K.; Fung, J. C. H. Abundance and Seasonal Characteristics of Elemental and Organic Carbon in Hong Kong PM10. *Atmos. Environ.* **2004**, *38* (10), 1511–1521.
- (47) Kwok, R. H. F.; Fung, J. C. H.; Lau, A. K. H.; Fu, J. S. Numerical Study on Seasonal Variations of Gaseous Pollutants and Particulate Matters in Hong Kong and Pearl River Delta Region. *J. Geophys. Res.: Atmos.* **2010**, *115* (D16), 012809.
- (48) Bergstrom, R. W.; Pilewskie, P.; Russell, P. B.; Redemann, J.; Bond, T. C.; Quinn, P. K.; Sierau, B. Spectral Absorption Properties of Atmospheric Aerosols. *Atmos. Chem. Phys.* **2007**, *7* (23), 5937–5943.
- (49) Saleh, R.; Hennigan, C. J.; McMeeking, G. R.; Chuang, W. K.; Robinson, E. S.; Coe, H.; Donahue, N. M.; Robinson, A. L. Absorptivity of Brown Carbon in Fresh and Photo-Chemically Aged Biomass-Burning Emissions. *Atmos. Chem. Phys.* **2013**, *13* (15), 7683–7693.
- (50) Kumar, N. K.; Corbin, J. C.; Bruns, E. A.; Massabó, D.; Slowik, J. G.; Drinovec, L.; Močnik, G.; Prati, P.; Vlachou, A.; Baltensperger, U.; Gysel, M.; El-Haddad, I.; Prévôt, A. S. H. Production of Particulate Brown Carbon during Atmospheric Aging of Residential Wood-Burning Emissions. *Atmos. Chem. Phys.* **2018**, *18* (24), 17843–17861.
- (51) Liu, J.; Lin, P.; Laskin, A.; Laskin, J.; Kathmann, S. M.; Wise, M.; Caylor, R.; Imholt, F.; Selimovic, V.; Shilling, J. E. Optical Properties and Aging of Light-Absorbing Secondary Organic Aerosol. *Atmos. Chem. Phys.* **2016**, *16* (19), 12815–12827.
- (52) Liu, P. F.; Abdelmalki, N.; Hung, H.-M.; Wang, Y.; Brune, W. H.; Martin, S. T. Ultraviolet and Visible Complex Refractive Indices of Secondary Organic Material Produced by Photooxidation of the Aromatic Compounds Toluene and m-Xylene. *Atmos. Chem. Phys.* **2015**, *15* (3), 1435–1446.
- (53) Wood, S. N.; Augustin, N. H. GAMs with Integrated Model Selection Using Penalized Regression Splines and Applications to Environmental Modelling. *Ecol. Model.* **2002**, *157* (2–3), 157–177.
- (54) Bauer, D. F. Constructing Confidence Sets Using Rank Statistics. *J. Am. Stat. Assoc.* **1972**, *67* (339), 687–690.
- (55) Xu, L.; Guo, H.; Boyd, C. M.; Klein, M.; Bougiatioti, A.; Cerully, K. M.; Hite, J. R.; Isaacman-VanWertz, G.; Kreisberg, N. M.; Knote, C.; Olson, K.; Koss, A.; Goldstein, A. H.; Hering, S. V.; de Gouw, J.; Baumann, K.; Lee, S.-H.; Nenes, A.; Weber, R. J.; Ng, N. L. Effects of Anthropogenic Emissions on Aerosol Formation from Isoprene and Monoterpenes in the Southeastern United States. *Proc. Natl. Acad. Sci. U.S.A.* 2015, 112 (1), 37–42.
- (56) Petzold, A.; Ogren, J. A.; Fiebig, M.; Laj, P.; Li, S.-M.; Baltensperger, U.; Holzer-Popp, T.; Kinne, S.; Pappalardo, G.; Sugimoto, N.; Wehrli, C.; Wiedensohler, A.; Zhang, X.-Y. Recommendations for Reporting "Black Carbon" Measurements. *Atmos. Chem. Phys.* **2013**, *13* (16), 8365–8379.